CONFORMATIONAL SIGNALS IN THE C-TERMINAL DOMAIN OF METHIONINE ADENOSYLTRANSFERASE I/III DETERMINE ITS NUCLEOCYTOPLASMIC DISTRIBUTION

Edel Reytor[1], Juliana Pérez-Miguelsanz[2], Luis Alvarez[3], Dolores Pérez-Sala[4] and María A. Pajares[1,5]

[1]Instituto de Investigaciones Biomédicas Alberto Sols (CSIC-UAM), Arturo Duperier 4, 28029 Madrid, Spain

[2]Departamento de Anatomía y Embriología Humana I, Facultad de Medicina, Universidad Complutense de Madrid, Plaza de Ramón y Cajal s/n, 28040 Madrid, Spain.

[3]Unidad de Investigación, Hospital Universitario La Paz, Paseo de la Castellana 261, 28046 Madrid, Spain.

[4]Centro de Investigaciones Biológicas (CSIC), Ramiro de Maeztu 9, 28040 Madrid, Spain

Short title: MAT I/III nuclear localization

[5]Address correspondence to: María A. Pajares, Instituto de Investigaciones Biomédicas Alberto Sols (CSIC-UAM), Arturo Duperier 4, 28029 Madrid, Spain (Phone: 34-915854414; FAX: 34-915854401; email: mapajares@iib.uam.es)

ABSTRACT

The methyl donor S-adenosylmethionine is synthesized in mammalian cytosol by three isoenzymes. Methionine adenosyltransferase II is ubiquitously expressed, whereas isoenzymes I (homotetramer) and III (homodimer) are considered the hepatic enzymes. In this work, we identified methionine adenosyltransferase I/III in most rat tissues both in the cytoplasm and the nucleus. Nuclear localization was the preferred distribution observed in extrahepatic tissues, where the protein colocalizes with nuclear matrix markers. A battery of mutants used in several cell lines to decipher the determinants involved in methionine adenosyltransferase subcellular localization demonstrated, by confocal microscopy and subcellular fractionation, the presence of two partially overlapping areas at the C-terminal end of the protein involved both in cytoplasmic retention and nuclear localization. Immunoprecipitation of coexpressed FLAG and EGFP fusions and gel filtration chromatography allowed detection of tetramers and monomers in nuclear fractions that also exhibited S-adenosylmethionine synthesis. Neither nuclear localization nor matrix binding required activity, as demonstrated with the inactive F251D mutant. Nuclear accumulation of the active enzyme only correlated with histone H3K27 trimethylation among the epigenetic modifications evaluated, therefore pointing to the necessity of methionine adenosyltransferase I/III to guarantee the supply of S-adenosylmethionine for specific methylations. However, nuclear monomers may exhibit additional roles.

Key words: S-adenosylmethionine synthetase, epigenetic modifications, structural determinants of localization, tissular expression, nuclear methylations.

INTRODUCTION

Control of gene expression and synthesis of adrenaline or phospholipids such as phosphatidylcholine are some examples of processes involving S-adenosylmethionine (AdoMet)-dependent methylations (1). AdoMet also participates in other important reactions such as those catalyzed by SAM radical proteins (i.e. biotin synthesis) or, upon decarboxylation, in spermidine and spermine synthesis (2, 3). In fact, all the radicals surrounding the AdoMet sulfur atom can be donated, as well as the carboxyl and amino groups of the methionine and the ribosyl moiety (4, 5). Thus, the number of processes involving AdoMet has been calculated to be as large as that of reactions using ATP. This small positively charged compound is synthesized from methionine and ATP in a singular reaction catalyzed by methionine adenosyltransferases (MATs)(6). These enzymes are present in the cytoplasm of eukaryotic cells (2), though reactions using this compound exhibit a wider subcellular distribution. Transfer of AdoMet to other cell compartments is therefore needed and carried out by specific transporters (7). Changes in AdoMet levels have been detected in several diseases, ranging from Parkinson (8) to alcohol liver cirrhosis (9). However, a direct correlation between AdoMet levels and pathology was only obtained by generating *MAT1A* knockout mice, which spontaneously develop hepatocellular carcinoma (HCC)(10).

Sequences for MAT catalytic subunits are highly conserved in all organisms (11), except in Archaea (12). This strong conservation is also observed at the structural level, with monomers composed by three domains formed by non-consecutive stretches of the sequence (13). General properties of these proteins include their association into oligomers to form the intersubunit active sites and their tripolyphosphatase activity. In mammals, three isoenzymes have been

detected, one ubiquitous (MAT II) and two others considered to be liver-specific (MAT I and III). MAT II is believed to be a heterotetramer $(\alpha 2\beta)_2$, where $\alpha 2$ is the catalytic subunit and β is the regulatory subunit, encoded by the *MAT2A* and *MAT2B* genes, respectively (14). On the other hand, MAT I is a homotetramer, and MAT III is a homodimer, of a $\alpha 1$ subunit that is 396 amino acids long and is codified by the *MAT1A* gene (2). These isoenzymes differ in their affinities for methionine, an important fact in human liver, where 48% of the ingested amino acid is metabolized (2). MAT I/III are the main forms in adult hepatocytes, whereas MAT II is the prevalent fetal enzyme (15). Moreover, the expression pattern is also altered in carcinogenesis (16, 17), during liver regeneration (18, 19), and after glucocorticoid stimulation (20). In addition, reductions in MAT I/III activity were shown in animal models of toxicity leading to GSH depletion (21, 22) or to enhancement of nitric oxide levels (23). Surprisingly, two patients expressing truncated MAT$\alpha 1$ subunits exhibit impaired hepatic MAT activity, together with neurological symptoms (24), thus suggesting a key role for MAT I/III in extrahepatic tissues. In order to shed light on these effects, we performed the present work, which describes the presence of MAT I/III in most tissues. The enzyme location to the cell nucleus and the structural features that contribute to subcellular localization are also identified. Moreover, the correlation of nuclear localization with specific methylation marks, whose alteration may lead to disease development, is demonstrated.

MATERIAL AND METHODS

Tissue extraction and hepatocyte isolation. Rat tissues were obtained from normal male Wistar rats (200 g). One portion was immediately frozen in liquid nitrogen for RNA isolation, and another was included in 4% (v/v) formaldehyde in PBS for immunohistochemistry. Fresh livers were used to obtain nuclear fractions and hepatocyte isolation with collagenase (Boehringer Mannheim, Mannheim, Germany) perfusion (25). Hepatocytes were suspended in Krebs-Henseleit medium with 10 mM glucose, and incubated at 37ºC with shaking in an O_2/CO_2 (95%/5%) gas phase. The viability was evaluated by the Trypan blue test; usually 90-95% cells excluded the stain. Normally, 3 $x10^5$ cells were seeded on coverslips and incubated for 4h in RPMI medium contaning 10% (v/v) FBS before fixation as described for the cell lines. All animals were treated according to the Guidelines for Animal Experimentation of the CSIC and the European Union.

RNA isolation and RT-PCR. Total RNA was isolated using the Tri-Reagent (Sigma Chemical Co, St. Louis, Mo, USA) and following the manufacturer's instructions. The primers used for RT-PCR were 5'-ATGGACCTGTGGATGGC-3' and 5'-TGGCCTCCAGTGTTATGT-3' for MAT1A and 5'-ATGAACGGGCAGCTCAA-3' and 5'-GCGTAACCAAGGCAATG-3' for MAT2A amplification, rendering fragments of 640 and 508 nucleotides, respectively. Reactions were performed using the Retrotools cDNA/DNA polymerase kit (Biotools, Madrid, Spain) for 30 cycles following the manufacturer's instructions. Real-time RT-PCR was performed using the 18S gene as reference, the MAT1A primers and conditions previously described (26).

Immunohistochemistry. For the detection of MATα1 on 5 μm thick paraffin sections, endogenous peroxidase activity was blocked by incubation in 2% (v/v) H_2O_2 in methanol for 10 minutes in the dark. Sections were heated in 1 mM EDTA for 45 minutes at 150ºC before incubation with 1% (w/v) BSA for 30 minutes. Immunostaining was obtained by incubation with anti-MAT antiserum (27) (1:1000, v/v) for 2 hours at room temperature followed by EnVision (DAKO Corporation, Carpinteria, CA, USA) incubation for 30 minutes using 3,3'-diaminobenzidine for color development following manufacturer's instructions. Counterstaining was performed with hematoxilin. For negative controls, the preimmune rabbit serum was used. Sections were photographed and analyzed using Adobe-Photoshop software.

Constructs and site-directed mutagenesis. Plasmids pSSRL-BlueT2 (27) and pSSRL-T7N (28) were used to obtain the MAT1A ORF for the new constructs that were named according to their main characteristics. pTRE-tight-MAT-EGFP for expression in a CHO-K1 Tet-On cell line (BD Biosciences, San Jose, CA, USA) was obtained by mutation of the MAT stop codon in pSSRL-Blue-T2 using the QuikChange method (Stratagene, La Jolla, CA, USA) (modified or included bases appear underlined), the primer 5'-GAAGCTTGTGTTTAGAGCCTCGAGTG-3' and its complement. The plasmid was then Kpn I/Bam HI digested, and the insert was ligated on pTRE-tight-EGFP (BD Biosciences, San Jose, CA, USA). This construct renders a fused MAT-EGFP protein including a 10 amino acid linker sequence at the C-terminal of MAT (RASSAGGSPR). pMAT-EGFP-T7N was prepared by Nde I/Eco RI digestion of pTRE-tight-MAT-EGFP and cloning of the corresponding fragment on pT7.7 for *E. coli* expression. pMAT-EGFP for expression of the fusion protein in nonregulated systems was obtained from pSSRL-Blue-T2 by Xho I/Hind III digestion with loss of the four C-terminal amino acids of MAT, two of which were recovered by cloning on pEGFP-N1 (BD

Biosciences, San Jose, CA, USA). This strategy creates a 17 amino acid linker at the C-terminal end of MAT with the sequence RILQSTVPRARDPPVAT.

pFLAG-MAT was prepared by cloning the MATα1 ORF, obtained by Eco RI/Bam HI digestion of pSSRL-BlueT2, into a modified pFLAG-CMV4 vector (Sigma Chemical Co, St. Louis, Mo, USA) including a Kpn I restriction site. To produce in frame FLAG-MAT, an additional base was introduced using the oligonucleotide 5'-CAAGCTTGCGGCACGCGAATTCATC-3' and its complement. The new fusion protein includes 15 extra amino acids in its N-terminus (MDYKDDDDKLDIEFH).

p(313-396)-EGFP5x and p(351-396)-EGFP5x, including the sequences encoding for the 313-396 and 351-396 protein fragments fused to EGFP pentamers, were prepared by PCR amplification of the corresponding regions of pSSRL-BlueT2 using the sense oligonucleotides 5´-CAGCTAGCATGCGGAGAGTCCTTGTTCAGGT-3’ and 5´-CAGCTAGCATGAACAAGAACTTTGACCTCCGG-3´, respectively and the antisense primer 5´-CAGCTAGCGCAAACACAAGCTTCTTGGGGA-3´. Primers include Nhe I sites for further cloning in pEGFP5x generously provided by Dr. Lazebnick (29). p(393-396)-EGFP5x was obtained by mixing 1.5 μg each of the oligonucleotides 5´-CTAGATGAAGCTTGTGTTTGCG-3´ (sense) and 5´-CTAGCGCAAACACAAGCTTCAT-3´ (antisense), including Nhe I sites, denaturation for 3 minutes at 95ºC, annealing by cooling to 25ºC in 46 minutes and phosphorylation prior to cloning in pEGFP5x. All the sense oligonucleotides designed for fragment expression include ATG initiation codons.

MAT mutants and truncated proteins were prepared using the QuikChange method and the mutagenic oligonucleotides included in Table 1, except for the F251D inactive mutant for

which the primers described previously were utilized (13). Mutations were verified by automatic sequencing.

Cell culture and transfections. CHO (ovary), N2a (neuroblastoma), COS-7 (kidney) and H35 (hepatoma) cell lines were grown in DMEM (Gibco, Carlsbad, CA, USA) supplemented with 10% (v/v) FBS and 2 mM glutamine, whereas HEK 293T cells (kidney) were cultured in the same medium using polyornithine (Sigma Chemical Co, St. Louis, Mo, USA)-coated plates. For CHO-K1 Tet-On culture, 10% (v/v) Tet system-approved FBS (BD Biosciences, San Jose, CA, USA) was used. Transfections were performed using Lipofectamine (Invitrogen, Carlsbad, CA, USA). Selection of stable clones was performed in the Tet-On system using 1-1.4 mg/ml hygromycin (BD Biosciences, San Jose, CA, USA) after 48 hours of culture. One of the stable clones showing doxycycline (BD Biosciences, San Jose, CA, USA)-dependent expression of MAT was called CHO Tet-On MAT-EGFP and was used in further studies.

Immunofluorescence. Direct immunofluorescence of both the CHO Tet-On stable clone (in the presence of doxycycline) and of the transient transfections (12000 cells on glass coverslips) was performed after 48 hours of culture. For indirect immunofluorescence, cells were fixed for 10 minutes with 2% (v/v) formaldehyde, permeabilized for 10 minutes with 0.3% (v/v) Triton X-100 and incubated for 30 minutes with 10% (v/v) FBS. Cells were then incubated for 1 hour at 37ºC with the monoclonal M2 anti-FLAG antibody (5 μg/ml; Sigma Chemical Co, St. Louis, Mo, USA) and later for 45 minutes at 37ºC with an antimouse secondary antibody conjugated to Alexa fluor 488 (1:800 v/v; Molecular Probes, Carlsbad, CA, USA). Glass coverslips were mounted using FluorSave™ reagent (Calbiochem, Darmstadt, Germany). Nuclei were stained using 5 μg/ml Hoechst 33342 dye (Molecular Probes, Carlsbad, CA, USA) for 1 hour before fixation or direct observation. Cell imaging (0.3-0.4 μm sections) was performed on

a Leica TCS SPII Spectral microscope using a 63x/1.3 NA objective. Images were analyzed using the Leica Confocal Software (LCS Lite, Zurich, Switzerland). Leptomycin B treatment (10 ng/ml; Calbiochem, Darmstadt, Germany) was performed for 6 hours before fixation or direct observation.

DNA methylation. The level of methylated DNA was followed by immunofluorescence using an anti 5-methyl cytosine antibody (1:1000; Calbiochem, Darmstadt, Germany) on fixed cells treated with 4 N HCl and 0.1 % (v/v) Triton X-100 for 30 minutes. Additionally, genomic DNA was isolated from transfected cells using the DNeasy kit (Qiagen, Hilden, Germany) and the incorporation of methyl groups from [^{3}H-methyl]-AdoMet (GE Healthcare, Barcelona, Spain) was followed by the radioactivity assay described by Christman et al. (30) using *E. coli* SssI methylase (New England Biolabs, Beverly, MA, USA).

Protein expression. Expression of MAT-EGFP in the Tet-On system was obtained by addition of doxycycline 0-4 μg/ml for two days. Protein expression in *E. coli* was obtained by transformation of competent BL21(DE3) cells. Constitutive FLAG-MAT expression was obtained after 12-16 hours of culture at 37ºC, whereas MAT-EGFP expression was induced at A_{595} of 0.3-0.4 with 0.5 mM IPTG (Ambion, Austin, TX, USA) for 3 hours at 37ºC.

Tissue and cell extracts. Cytosolic fractions of the tissues (20), cell cultures (31) and bacteria (28) for activity, western blot and gel filtration measurements were prepared as previously described. Separation of nuclear and cytosolic fractions for western blot was carried out as described previously (32), whereas for MAT activity measurements detergents were eliminated (33). Evaluation of histone methylation was carried out in cell extracts obtained by 30 minute incubation on ice in 50 mM Tris/HCl pH 7.5, 150 mM NaCl, 0.5% (v/v) SDS, 30 mM

sodium pyrophosphate, 50 mM NaF and protease inhibitors, followed by centrifugation at 100000 x g 30 minutes.

Nuclear matrix preparation. Cells grown on coverslips (12 mm) were fixed with 2% (v/v) formaldehyde for 10 minutes, washed with PBS and incubated with CSK buffer (10 mM Pipes pH 6.8, 100 mM NaCl, 1 mM EGTA, 3 mM $MgCl_{2,}$ 300 mM sucrose) containing 0.5 % (v/v) Triton X-100 for 15 minutes. This solution was replaced by CSK buffer including 1% (v/v) NP-40 and 0.5% (w/v) sodium deoxycholate for 15 minutes, followed by a 1 minute treatment with 300 mM imidazole. Chromatin elimination was performed by RNAse-free/DNAse treatment (500 U/ml; Roche, Indianapolis, IN, USA) in CSK buffer for 1 hour at 37ºC, followed by 2 minutes incubation with 250 mM ammonium sulfate, and 1 minute with 2M NaCl in CSK buffer without sucrose and fixation with 3.7% (v/v) formaldehyde for 10 minutes before immunostaining.

Gel filtration chromatography. Samples of bacterial (1-2 mg) or eukaryal cytosols (1 mg) and nuclear extracts (0.5 mg) were injected on a Superose 12 HR 10/30 gel filtration column (GE Healthcare, Barcelona, Spain), and elution, MAT activity measurements (100 µl) and Dot-Blot analysis (10 µl) were performed as previously described (34).

SDS-PAGE electrophoresis and immunoblotting. Denaturing gel electrophoresis was performed on 10% SDS-PAGE gels under reducing conditions, using the Laemmli buffer system. Samples containing 80, 40 or 5 µg of tissue, cellular or bacterial cytosols, respectively, were loaded per lane. Histone methylation was detected using 10 µg/lane of cell extracts. Immunoblotting analysis was carried out as described previously (27) using anti-MAT (1:10000), anti-FLAG (5 µg/ml; Sigma Chemical Co, St. Louis, Mo, USA), anti-EGFP (1:5000; BD Biosciences, San Jose, CA, USA), anti-cJun (1:1500; Santa Cruz), anti-TBP (1:1000; Santa

Cruz Biotechnology, SantaCruz, CA, USA), anti-α-Tubulin (1:10000; Sigma Chemical Co, St. Louis, Mo, USA), anti-trimethyl H3K4 (0.1 μg/ml; Upstate, Charlottesville, VA, USA), anti-trimethyl H3K9 (1:2000; Upstate, Charlottesville, VA, USA) or anti-trimethyl H3K27 (1 μg/ml; Upstate, Charlottesville, VA, USA) antibodies, as required. Protein bands were visualized using Western Lightning™ chemiluminescence reagent (Perkin Elmer, Waltham, MA, USA).

Immunoprecipitation. Nuclear and cytoplasmic fractions (400 μl) were incubated o/n at 4ºC with anti-FLAG M2 Affinity Gel (40 μl; Sigma Chemical Co, St. Louis, Mo, USA). After three washes using TBS, the samples were boiled 10 minutes in Laemmli sample buffer including 100 mM DTT, microfuged for 1 minute at 10000 x g and the supernatants loaded onto SDS-PAGE gels.

Determination of methionine adenosyltransferase and LDH activities. MAT activity was measured as described by Gil et al. (20) using 160 μl of cytosolic samples or 100 μl of gel filtration fractions and 5 mM concentrations of both ATP and methionine. Detection of activity in the nuclear fractions was performed for up to 2 hours with a 4 Ci/mol reaction mixture. LDH activity was measured at 340 nm and 37ºC for 5 min using 10-100 μl of the subcellular fractions in 50 mM Tris/HCl pH 7.5, 0.2 mM NADH (Sigma Chemical Co, St. Louis, Mo, USA) and 1 mM pyruvate (Sigma Chemical Co, St. Louis, Mo, USA).

Protein concentration determination. The protein concentration of the samples was measured using the Bio-Rad protein assay kit and bovine serum albumin as the standard.

Sequence analysis and molecular modeling. Analysis of the MATα1 sequence in the search for putative localization and export signals was performed using the programs NetNES (35) and PredictNLS (36) and the PSort II server, whereas for molecular modeling, the Swiss-PdbViewer (Glaxo Smithkline R & D) was used.

Statistical analysis. Student's t-test for unpaired samples was applied for statistical analysis using GraphPad Prism v. 5.0 (GraphPad Software, San Diego). Differences were considered significant when $p < 0.05$.

RESULTS

Expression of MAT1A RNA and MATα1 protein shows a wide distribution. MATα1 was detected in the cytosol of all rat tissues examined by western blot using an anti-MAT I/III polyclonal antiserum. The liver protein signal was the strongest, and the signals of heart, lung and skeletal muscle showed the lowest levels (Fig. 1A). Notably, a double band was consistently observed in all extrahepatic tissues. The same anti-MAT antiserum was used for immunohistochemistry, and again, signals for MAT I/III were detected in all the tissues tested, except in endothelium, smooth muscle and connective tissue of the visceral walls (Fig. 1B and Table 2). Among the cell types clearly labeled, hepatocytes, Purkinje cells, renal tubule, bronchiolar and spermatogenic epithelial cells and pancreatic acinar cells could be identified. In contrast to the generally accepted cytoplasmic distribution of the protein, nuclear staining was a general feature observed in the nonhepatic cells, but also in hepatocytes. Moreover, the strongest liver signals were detected in the periportal area with a decreasing gradient of staining towards the perivenous area (Fig. S1). Confirmation of the broad expression of MAT1A was obtained by RT-PCR using total RNA purified from the same rat tissues in combination with specific oligonucleotides for MAT1A or MAT2A amplification (Fig. 1C). All the samples showed signals corresponding to both cDNAs, except for aorta, which only showed MAT2A signal. Controls performed using these primers and plasmids including ORFs for MAT1A and MAT2A

demonstrated their specificity (data not shown). Real-time PCR quantification confirmed the highest MAT1A expression in liver, demonstrated intermediate levels in lung, pancreas and kidney and faint signals in the rest of the tissues tested (Fig. 1D). Thus, expression of MAT1A can no be longer considered liver specific.

MATα1 localizes to cytoplasm and nucleus. In order to confirm the subcellular distribution observed by immunohistochemistry, several MAT constructs were prepared, and their behavior was analyzed in various cell lines by confocal fluorescence microscopy. The constructs include tags at the N- (FLAG-MAT) or C-terminal ends (MAT-EGFP) of the MATα1 ORF, respectively (Fig. 2A). Western blot analysis showed expression of the proteins in bacterial and cellular extracts with the expected mobilities: 48 kDa (wild type MATα1), 50 kDa (FLAG-MAT) and 78 kDa (MAT-EGFP)(Fig. 2B). All constructs were active and retained oligomerization capacity upon expression in *E. coli* (Table 3), but their expression level was much lower than that of the wild type protein. The association state of the fusion proteins was found to be dimeric by gel filtration chromatography (150 and 90 kDa for MAT-EGFP and FLAG-MAT, respectively), which is the minimum required for catalysis. Peaks for the controls containing *E. coli* MAT appeared in volumes corresponding to approximately 180 kDa, and hence their activity profiles partially overlap with MAT-EGFP and FLAG-MAT (data not shown). Precise identification of the elution position was obtained by Dot blot using anti-MAT I/III antiserum. Thus, the fusion forms of MAT I/III are active oligomers, their sizes being larger than that required for diffusion through the nuclear pore.

Transient transfections of both FLAG-MAT and MAT-EGFP constructs were analyzed in several cell lines (CHO-K1, N2a, COS-7, H35 and HEK 293T), in addition to a stable doxycycline-inducible MAT-EGFP clone prepared in CHO cells. In all cases, cells demonstrated

strong cytoplasmic fluorescence along with a lighter nuclear signal that overlapped with Hoechst staining (Fig. 3A). The use of the stable clone allowed detection in cytoplasmic and nuclear compartments independently of the expression levels, thus indicating that nuclear localization of exogenous MAT is not due to saturation effects (Fig. 3B). Moreover, the nuclear MAT signal was excluded from presumptive nucleoli. The results obtained by *in vivo* and indirect fluorescence were consistent, thus excluding artifacts due to cell fixation or the influence of the tag localization in the protein structure. Indirect immunofluorescence of isolated hepatocytes showed a similar distribution pattern to that observed in the cell lines and by immunohistochemistry (Fig. 3C). In addition, subcellular fractionation followed by western blot analysis confirmed the presence of MATα1 subunits in the nuclear and cytosolic fractions of several cell lines (Fig. 3D). The purity of these fractions was assessed by detection of cJun and α-Tubulin as nuclear and cytoplasmic markers, respectively. Therefore, our results confirm the nuclear localization of MATα1 as a general feature in all cell types used.

Analysis of MATα1 sequence and structure in search for localization determinants. Commonly, transport to different subcellular compartments is dependent on the presence of protein targeting signals, and several programs have been developed to search for the presence of this type of sequences in any given protein. Among them, we have analyzed the MATα1 sequence using NetNES, PredictNLS and PSort II, none of which identified nuclear export (NES) or localization signals (NLS) in this protein. Only a stretch at the C-terminal end of the protein comprising V360-L367 showed a low score for a possible NES, but NetNES considered it to be below its confidence levels. In fact, addition of the CRM1 (exportin 1) inhibitor leptomycin B to the transfected cells induced no changes in MATα1 distribution (data not shown). These results

do not support the presence of classical signals of transport, but they do not exclude other mechanisms or other determinants of localization.

Classical NLSs include sequences rich in basic residues placed at certain distances, which can be resembled structurally. The MATα1 sequence contains a considerable number of lysine and arginine residues at the C-terminal end (16.7% of the last 96 amino acids). Some of these residues appear paired and exposed at the protein surface (Figs. 2C,D), outside of the oligomerization interfaces. A first approach to check for the possible implication of this part of the molecule in subcellular localization was to prepare C-terminal deletions on FLAG-MAT (Fig. 2C). These truncated forms correspond to proteins lacking: 1) the last four residues, including one of the lysines in the last basic pair (FLAG-MAT K393X); 2) 80% of the C-terminal domain including most of the C-terminal basic sequence (FLAG-MAT R313X); and 3) half of this basic area (FLAG-MAT N351X). Truncated proteins were expressed in both *E. coli* and the mammalian cell lines used in this study, and their production was confirmed by the detection of bands with the expected mobilities (39.5, 44 and 50 kDa)(Fig. 4A). Determination of their oligomeric association state was precluded due to the reduced expression levels attained, and the low MAT activity that was measured (Table 3). Confocal microscopy and subcellular fractionation revealed nuclear accumulation of the three truncated proteins as compared to the control (Figs. 4A,B and supplemental data Tables S1, S2). These results suggest that the C-terminal domain of MATα1 is involved in cytoplasmic retention, but the existence of a NLS in the truncated protein or exposure of a NLS otherwise buried in the subunit structure cannot be excluded (supplemental data Fig. S2). To distinguish among these possibilities the fragments deleted were fused to EGFP5x, and their behavior was analyzed (Fig. 4C). The size of these fusion proteins precluded diffusion through the nuclear pore, and hence they would be retained

in the cytoplasm, unless these fragments included signals for targeting to a different subcellular location. *In vivo* fluorescence revealed cytoplasmic accumulation in all the cases as compared to EGFP5x and NLS-tagged EGFP3x, and in contrast to the behavior of the truncated proteins. Thus, the involvement of MATα1 C-terminus in cytoplasmic retention seems feasible.

In parallel, the role of the basic residues at the C-terminal domain was explored by point mutation, an approach that induced minimum structural perturbations. For this purpose, only those lysine or arginine residues exposed at the protein surface were selected for alanine substitution (Fig. 2D). Mutants were prepared in both FLAG-MAT and MAT-EGFP plasmids in order to avoid artifacts due to either fixation or masking by the fusion of EGFP (27 kDa). All the mutants exhibited MAT activity and were able to oligomerize as studied in *E. coli* overexpressing extracts, their dimer/tetramer ratio depending on the protein concentration as previously described for wild type MAT I/III (Table 3). Confocal fluorescence microscopy revealed that mutations at positions 313, 340, 341, 344, 368, 369, 392 and 393 elicited similar behavior of both constructs (Fig. 5A). A reduction in nuclear MATα1 content was observed for K340A, K341A, R344A and K393A that was especially clear for R344A and K393A, whereas R313A, K368A, K369A and K392A tended to accumulate in the nucleus (Fig. 5A and supplemental data Table S1). Subcellular fractionation of the total culture confirmed this behavior for most of the mutants (Fig. 5B and supplemental data Table S2). Thus, looking at the subunit structure (Fig. 2D), mutants related to nuclear localization are next to those involved in cytosolic retention. Notably, whereas K393A accumulates in the cytoplasm, deletion of the 393-396 stretch resulted in increased nuclear signal, therefore highlighting the role of residues 394-396 in cytosolic retention. Moreover, the behavior exhibited by the K392A mutant also corresponds to a cytosolic retention signal, hence pointing to a possible overlap between areas

involved in cytosolic retention and nuclear localization at the C-terminal end of the MATα1 chain. Thus, nuclear localization is related to the triangular area comprised by residues 340, 344 and 393 (including 341), whereas cytoplasmic retention is determined by the area delimited by residues 313, 368, 369 and 392 that shows partial spatial overlap at K393 and the 394-396 stretch (Fig. 2D). These results suggested the presence of structural rather than sequence-based localization determinants in MATα1 subunits.

MATα1 subunits localize to the nuclear matrix. Confocal microscopy showed the exclusion of MATα1 from the nucleoli in all the cell lines tested (Fig. 3A). To get further insight into the precise subnuclear distribution, CHO and COS-7 cells were transfected with pFLAG-MAT, fixed and extracted with detergents and high salt in order to obtain the nuclear matrix. Indirect immunofluorescence showed the presence of MATα1 at nuclear speckles as shown by colocalization with signals of an anti-SC35 antibody (Fig. 6). Additionally, other constructs used in this study were also checked for their putative association to the nuclear matrix. The results indicated that none of the C-terminal deletions precluded nuclear matrix association, and hence suggested that determinants for this binding may be located in other domains of the protein.

Nuclear MATα1 association state and effects on specific methylations. Two different association levels of MATα1 subunits have been described in the cytoplasm: tetramers and dimers. The nuclear localization of MATα1 subunits may or may not be related to AdoMet synthesis, for which oligomerization is needed. In order to clarify this point, cotransfections using FLAG-MAT and MAT-EGFP were performed, and the nuclear and cytoplasmic fractions were isolated. Expression was demonstrated in the input fractions by western blot with anti-FLAG and anti-EGFP antibodies, and the purity of the subcellular fractions was assessed with anti-cJun and anti-α-Tubulin antibodies and LDH activity (Fig. 7A). Nuclear and cytosolic

fractions were immunoprecipitated with anti-FLAG Affinity Gel and the immunoprecipitates were further analyzed by western blot with an anti-EGFP antibody. The presence of a band showing the correct size for MAT-EGFP suggested that MATα1 subunits appear as oligomers in the nucleoplasm, and hence preserve AdoMet synthesizing capacity. Controls cotransfected with pFLAG-MAT and pEFGP showed no EGFP signal in the immunoprecipitates, thus confirming the MAT-MAT interaction specificity. Nuclear extracts prepared without detergents exhibited low MAT activity (12.11 ± 3.18 pmol/min/mg) (Fig S3), as expected from the low proportion of oligomers and the large amount of monomers detected by gel filtration chromatography (Fig. 7B). Measurements of nuclear AdoMet concentrations were precluded due both to the low levels of the compound in this compartment and the long subcellular fractionation process that did not guarantee its preservation.

In order to get insight into the function of MATα1 in the nuclear compartment, the effect of different constructs on nuclear methylations was evaluated. Overexpression of FLAG-MAT produced significant increases in histone H3 trimethylation levels at positions K4, K9 and K27 (Fig. 8A), as well as in DNA methylation (supplemental data Fig. S4). These effects were not observed upon transfection of the inactive mutant F251D, although it was also distributed among the cytoplasm and nucleus as shown by both confocal microscopy and subcellular fractionation (Figs. 5A,B) and it retained nuclear matrix binding capacity (Fig. 6). Moreover, only K27me3 methylation levels correlated with the preferred subcellular distribution of the mutants (Fig. 8B and supplemental data Fig. S4). Hence, cells transfected with mutants with primary nuclear distribution (K368A and K369A) showed increased H3K27me3 (~2 fold), whereas those expressing mutants of preferred cytoplasmic location (R344A and K393A) exhibited levels comparable to those of the wild type protein. In addition, expression of the inactive F251D

mutant further reduced these specific methylation levels to those of the mock transfected cells. The results thus suggested that nuclear MATα1 is in its active oligomeric assembly in order to contribute to specific methylations, although preservation of the AdoMet synthesizing capacity is not a prerequisite for nuclear localization.

DISCUSSION

Mammalian MAT activity has been shown to be ubiquitous, but much higher in liver than in any other tissue. This fact was ascribed to the presence of specific hepatic isoenzymes known as MAT I and III. However, this specificity was questioned when their presence in the pancreas was reported (37). Now we show that the distribution of these isoenzymes is nearly ubiquitous in normal rat tissues. The presence of a double band in western blots of extrahepatic tissues may indicate a certain degree of cross-reactivity of the antibody used with MATα2, although no such pattern was previously reported (20, 27, 31). Attempts to detect MAT1A mRNA by northern blot in extrahepatic tissues failed previously (38), and hence we used specific primers against either of the catalytic MAT subunits and RT-PCR. The data further demonstrated a wider expression pattern for MAT1A, resembling that of western blot and immunohistochemistry experiments. Moreover, detection of MATα1 in extrahepatic tissues showed staining of the nuclear compartment, an observation that was later confirmed in several cell lines overexpressing two types of fusion proteins and in normal hepatocytes. Additionally, the large hepatic AdoMet production (~8 g/day in humans) requires a constant supply of ATP (2), which is consistent with a greater periportal distribution of the protein, correlating to the more aerobic hepatic areas, where oxidative energy metabolism takes place (39).

Analysis of the MATα1 sequence showed no evidence of classical mono- or bipartite NLSs (40). However, this fact does not exclude the existence of other less known determinants such as hydrophobic rich (41, 42), conformationally dependent (43-45) and PY NLSs (46), or piggyback transport mechanisms (47). The fact that several sets of paired basic residues occur at the C-terminal end of the protein led us to focus on this part of the molecule. The use of truncated MATα1 subunits and fusion of these fragments to multiple EGFP reporters confirmed the importance of this segment in subcellular localization. However, the fact that MAT domains are formed from nonconsecutive stretches of the sequence makes independent folding unfeasible (13), and hence the structure and folding of the truncated subunits (especially R313X and N351X), as well as the folding of the fragments, could differ strongly from those in the native protein. In addition, it should be noted that in many cases redundant NLSs have been observed (48) and the importance of the protein context in which these signals are placed (49). To overcome these problems, single mutants of exposed basic residues at the C-terminal were studied, and their behavior allowed discrimination of two areas with opposite character. One, delimited by residues 340-341-344-393, is involved in nuclear transport and another, 313-368-369-392, is involved in cytoplasmic retention. The high conservation observed in these residues among vertebrate MATs highlights the importance of this part of the structure and its role, the exceptions being K340 and the presence in MATα2 of an additional basic residue in the 392-396 stretch.

Although the sets of residues determining localization are scattered along the C-terminal domain sequence, they are placed close in the three-dimensional structure of the monomers, thus raising the possibility of a topological distribution similar to that of classical NLSs (43, 50). However, this does not seem to be the case for MATα1, as distances between analogous

positions differ by 2-10 Å. Areas determining cytosolic or nuclear MATα1 localization partially overlap in the structure, and hence the function of either one may be regulated by post-translational modification or interaction with partners that are unknown. Modification by nitric oxide is among the known mechanisms to act on NLSs (51) and is known to occur on MATα1 in vivo (23). However, nitrosylation occurs on cysteine 121 located at the loop of access to the active site, out of the C-terminal domain (23), and hence of the areas related to subcellular localization. The existence of other post-translational modifications on this enzyme has not been studied in vivo, although in vitro phosphorylation at T342 has been shown (52). On the other hand, cytosolic retention determinants are not well characterized and no consensus sequences have been postulated. In our case, the data allow us to define areas, including nonconsecutive stretches of the C-terminal domain, as being responsible for both nuclear and cytoplasmic localization, thus suggesting conformational determinants.

The role of MAT isoenzymes in AdoMet synthesis and the need of this metabolite for methylation of nuclear components may be linked to the presence of MATα1 in that compartment. The positive correlation among nuclear localization of MAT⟨1 oligomers, the active form of the enzyme, and trimethylation of histone H3K27 suggests its role to guarantee an adequate supply of the methyl donor for specific modifications, which is further supported by the results with the inactive mutant (F251D). This specificity could arise from the different affinities for AdoMet among histone and DNA methyltransferases. Although the small size of AdoMet, and even its positive charge, may not preclude diffusion through the nuclear pore (53), the possibility exists that its high instability requires in situ synthesis for gene repression, a process traditionally related to H3K27 trimethylation (54). Normal development depends on maintenance of the correct methylation pattern, whereas tumor progression is associated with aberrant

methylation (55). Thus, situations in which AdoMet levels are reduced may lead to disease development, as has been demonstrated in animals fed methionine-deficient diets (56, 57) and *MAT1A* knockout mice (10), in which hepatitis and HCC occur. In these models, as well as in pancreatitis (37), a switch between MAT1A and MAT2A expression is detected that is not enough to cope with all the AdoMet needs of the cell, suggesting a specific role for MAT I/III in epigenetic modification. This effect could acquire additional importance if, in spite of their high homology (11), MATα2 cannot substitute for the nuclear role of MATα1 in gene repression. Such a potential specific function is further supported by the minimal MATα1 expression detected in most tissues, where the protein is mainly nuclear.

Proteins involved in intermediary metabolism have been identified in the nucleus, although their role in this compartment has not always been established. Among them is S-adenosylhomocysteine hydrolase, whose nuclear presence has been ascribed to the need for S-adenosylhomocysteine removal during cap methylation to avoid inhibition of these reactions (58). However, other examples link nuclear location to the ability of the proteins to exhibit additional functions (moonlighting), properties that can be acquired, e.g. by oligomer dissociation (59). Detection of nuclear MATα1 as tetramers suggests its role in AdoMet synthesis, although the large amount of monomers may be related to the capacity to display other functions. Monomer structure should differ strongly from that of monomers in active oligomers, since the large hydrophobic surface of contact between subunits should be hidden from the solvent. Such a structural change provides new interaction possibilities that may be related to pathways other than those involving methylations. Such a new function opens new possibilities to explain the demyelination observed in the few patients expressing truncated MATα1 forms ~350 residues long. These neurological symptoms were ascribed previously to a reduction in

AdoMet levels due to hetero-oligomerization with MATα2, although these effects were difficult to conciliate with the hepatic expression of the enzyme (24).

In summary, our western and RT-PCR data show MAT1A expression in almost every tissue. Immunohistochemistry and overexpression of the protein also demonstrate its nuclear localization, offering additional possibilities to understand its pathological role. Overlapping regions responsible for nuclear and cytoplasmic localization are identified by mutagenesis of the C-terminal end of MAT I/III. Moreover, the preferred subcellular localization of the mutants correlates with changes in specific epigenetic methylations, effects that could depend directly on nuclear AdoMet synthesis or on other putative new functions of nuclear MATα1 monomers.

REFERENCES

1. Cantoni, G. L. (1975) Biological methylation: selected aspects. *Annu. Rev. Biochem.* **44**, 435-451

2. Mato, J. M., Alvarez, L., Ortiz, P., and Pajares, M. A. (1997) S-adenosylmethionine synthesis: molecular mechanisms and clinical implications. *Pharmacol. Ther.* **73**, 265-280

3. Fontecave, M., Mulliez, E., and Ollagnier-de-Choudens, S. (2001) Adenosylmethionine as a source of 5'-deoxyadenosyl radicals. *Curr. Opin. Chem. Biol.* **5**, 506-511

4. Dolnick, B. J., Angelino, N. J., Dolnick, R., and Sufrin, J. R. (2003) A novel function for the rTS gene. *Cancer Biol. Ther.* **2**, 364-369

5. Van Lanen, S. G., Kinzie, S. D., Matthieu, S., Link, T., Culp, J., and Iwata-Reuyl, D. (2003) tRNA modification by S-adenosylmethionine:tRNA ribosyltransferase-isomerase. Assay development and characterization of the recombinant enzyme. *J. Biol. Chem.* **278**, 10491-10499

6. Chiang, P. K., and Cantoni, G. L. (1977) Activation of methionine for transmethylation. Purification of the S-adenosylmethionine synthetase of bakers' yeast and its separation into two forms. *J. Biol. Chem.* **252**, 4506-4513

7. Horne, D. W., Holloway, R. S., and Wagner, C. (1997) Transport of S-adenosylmethionine in isolated rat liver mitochondria. *Arch. Biochem. Biophys.* **343**, 201-206

8. Cheng, H., Gomes-Trolin, C., Aquilonius, S. M., Steinberg, A., Lofberg, C., Ekblom, J., and Oreland, L. (1997) Levels of L-methionine S-adenosyltransferase activity in erythrocytes and concentrations of S-adenosylmethionine and S-adenosylhomocysteine in whole blood of patients with Parkinson's disease. *Exp. Neurol.* **145**, 580-585

9. Lu, S. C., Huang, Z. Z., Yang, H., Mato, J. M., Avila, M. A., and Tsukamoto, H. (2000) Changes in methionine adenosyltransferase and S-adenosylmethionine homeostasis in alcoholic rat liver. *Am. J. Physiol. Gastrointest. Liver Physiol.* **279**, G178-185

10. Lu, S. C., Alvarez, L., Huang, Z. Z., Chen, L., An, W., Corrales, F. J., Avila, M. A., Kanel, G., and Mato, J. M. (2001) Methionine adenosyltransferase 1A knockout mice are predisposed to liver injury and exhibit increased expression of genes involved in proliferation. *Proc. Nat. Acad. Sci. USA* **98**, 5560-5565

11. Sanchez-Perez, G. F., Bautista, J. M., and Pajares, M. A. (2004) Methionine adenosyltransferase as a useful molecular systematics tool revealed by phylogenetic and structural analyses. *J. Mol. Biol.* **335**, 693-706

12. Graham, D. E., Bock, C. L., Schalk-Hihi, C., Lu, Z. J., and Markham, G. D. (2000) Identification of a highly diverged class of S-adenosylmethionine synthetases in the archaea. *J. Biol. Chem.* **275**, 4055-4059

13. Gonzalez, B., Pajares, M. A., Hermoso, J. A., Alvarez, L., Garrido, F., Sufrin, J. R., and Sanz-Aparicio, J. (2000) The crystal structure of tetrameric methionine adenosyltransferase from rat liver reveals the methionine-binding site. *J. Mol. Biol.* **300**, 363-375

14. Kotb, M., and Geller, A. M. (1993) Methionine adenosyltransferase: structure and function. *Pharmacol. Ther.* **59**, 125-143

15. Gil, B., Casado, M., Pajares, M. A., Bosca, L., Mato, J. M., Martin-Sanz, P., and Alvarez, L. (1996) Differential expression pattern of S-adenosylmethionine synthetase isoenzymes during rat liver development. *Hepatology* **24**, 876-881

16. Cai, J., Sun, W. M., Hwang, J. J., Stain, S. C., and Lu, S. C. (1996) Changes in S-adenosylmethionine synthetase in human liver cancer: molecular characterization and significance. *Hepatology* **24**, 1090-1097

17. Cai, J., Mao, Z., Hwang, J. J., and Lu, S. C. (1998) Differential expression of methionine adenosyltransferase genes influences the rate of growth of human hepatocellular carcinoma cells. *Cancer Res.* **58**, 1444-1450

18. Huang, Z. Z., Mao, Z., Cai, J., and Lu, S. C. (1998) Changes in methionine adenosyltransferase during liver regeneration in the rat. *Am. J. Physiol.* **275**, G14-21

19. Frago, L. M., Gimenez, A., Rodriguez, E. N., and Varela-Nieto, I. (1998) Pattern of methionine adenosyltransferase isoenzyme expression during rat liver regeneration after partial hepatectomy. *FEBS Lett.* **426**, 305-308

20. Gil, B., Pajares, M. A., Mato, J. M., and Alvarez, L. (1997) Glucocorticoid regulation of hepatic S-adenosylmethionine synthetase gene expression. *Endocrinology* **138**, 1251-1258

21. Corrales, F., Ochoa, P., Rivas, C., Martin-Lomas, M., Mato, J. M., and Pajares, M. A. (1991) Inhibition of glutathione synthesis in the liver leads to S-adenosyl-L-methionine synthetase reduction. *Hepatology* **14**, 528-533

22. Corrales, F., Gimenez, A., Alvarez, L., Caballeria, J., Pajares, M. A., Andreu, H., Pares, A., Mato, J. M., and Rodes, J. (1992) S-adenosylmethionine treatment prevents carbon tetrachloride-induced S-adenosylmethionine synthetase inactivation and attenuates liver injury. *Hepatology* **16**, 1022-1027

23. Avila, M. A., Mingorance, J., Martinez-Chantar, M. L., Casado, M., Martin-Sanz, P., Bosca, L., and Mato, J. M. (1997) Regulation of rat liver S-adenosylmethionine synthetase during septic shock: role of nitric oxide. *Hepatology* **25**, 391-396

24. Chamberlin, M. E., Ubagai, T., Mudd, S. H., Wilson, W. G., Leonard, J. V., and Chou, J. Y. (1996) Demyelination of the brain is associated with methionine adenosyltransferase I/III deficiency. *J. Clin. Invest.* **98**, 1021-1027

25. Felíu, J. E., Hue, L., and Hers, H. G. (1976) Hormonal control of pyruvate kinase and gluconeogenesis in isolated rat hepatocytes. *Proc. Natl. Acad. Sci. USA* **73**, 2762-2766

26. Delgado, M., Perez-Miguelsanz, J., Garrido, F., Rodriguez-Tarduchy, G., Perez-Sala, D., and Pajares, M. A. (2008) Early effects of copper accumulation on methionine metabolism. *Cell. Mol. Life Sci.* **65**, 2080-2090

27. Mingorance, J., Alvarez, L., Sanchez-Gongora, E., Mato, J. M., and Pajares, M. A. (1996) Site-directed mutagenesis of rat liver S-adenosylmethionine synthetase. Identification of a cysteine residue critical for the oligomeric state. *Biochem. J.* **315**, 761-766

28. Alvarez, L., Mingorance, J., Pajares, M. A., and Mato, J. M. (1994) Expression of rat liver S-adenosylmethionine synthetase in Escherichia coli results in two active oligomeric forms. *Biochem. J.* **301**, 557-561

29. Faleiro, L., and Lazebnik, Y. (2000) Caspases disrupt the nuclear-cytoplasmic barrier. *J. Cell Biol.* **151**, 951-959

30. Christman, J. K., Weich, N., Schoenbrun, B., Schneiderman, N., and Acs, G. (1980) Hypomethylation of DNA during differentiation of Friend erythroleukemia cells. *J. Cell Biol.* **86**, 366-370

31. Sanchez-Gongora, E., Pastorino, J. G., Alvarez, L., Pajares, M. A., Garcia, C., Vina, J. R., Mato, J. M., and Farber, J. L. (1996) Increased sensitivity to oxidative injury in chinese hamster ovary cells stably transfected with rat liver S-adenosylmethionine synthetase cDNA. *Biochem. J.* **319**, 767-773

32. Cernuda-Morollon, E., Pineda-Molina, E., Canada, F. J., and Perez-Sala, D. (2001) 15-Deoxy-Delta 12,14-prostaglandin J2 inhibition of NF-kappaB-DNA binding through covalent modification of the p50 subunit. *J. Biol. Chem.* **276**, 35530-35536

33. Andrews N. C., and Faller D. V. (1991) A rapid micropreparation technique for extraction of DNA-binding proteins from limiting numbers of mammalian cells. *Nucleic Acid Res.* **19**, 2499

34. Sanchez-Perez, G. F., Gasset, M., Calvete, J. J., and Pajares, M. A. (2003) Role of an intrasubunit disulfide in the association state of the cytosolic homo-oligomer methionine adenosyltransferase. *J. Biol. Chem.* **278**, 7285-7293

35. la Cour, T., Kiemer, L., Molgaard, A., Gupta, R., Skriver, K., and Brunak, S. (2004) Analysis and prediction of leucine-rich nuclear export signals. *Protein Eng. Des. Sel.* **17**, 527-536

36. Cokol, M., Nair, R., and Rost, B. (2000) Finding nuclear localization signals. *EMBO Rep.* **1**, 411-415

37. Lu, S. C., Gukovsky, I., Lugea, A., Reyes, C. N., Huang, Z. Z., Chen, L., Mato, J. M., Bottiglieri, T., and Pandol, S. J. (2003) Role of S-adenosylmethionine in two experimental models of pancreatitis. *FASEB J.* **17**, 56-58

38. Alvarez, L., Asuncion, M., Corrales, F., Pajares, M. A., and Mato, J. M. (1991) Analysis of the 5' non-coding region of rat liver S-adenosylmethionine synthetase mRNA and comparison of the Mr deduced from the cDNA sequence and the purified enzyme. *FEBS Lett.* **290**, 142-146

39. Jungermann, K., and Kietzmann, T. (1996) Zonation of parenchymal and nonparenchymal metabolism in liver. *Annu. Rev. Nutr.* **16**, 179-203

40. Robbins, J., Dilworth, S. M., Laskey, R. A., and Dingwall, C. (1991) Two interdependent basic domains in nucleoplasmin nuclear targeting sequence: identification of a class of bipartite nuclear targeting sequence. *Cell* **64**, 615-623

41. Chen, M. H., Ben-Efraim, I., Mitrousis, G., Walker-Kopp, N., Sims, P. J., and Cingolani, G. (2005) Phospholipid scramblase 1 contains a nonclassical nuclear localization signal with unique binding site in importin alpha. *J. Biol. Chem.* **280**, 10599-10606

42. Polizotto, R. S., and Cyert, M. S. (2001) Calcineurin-dependent nuclear import of the transcription factor Crz1p requires Nmd5p. *J. Cell Biol.* **154**, 951-960

43. Sessler, R. J., and Noy, N. (2005) A ligand-activated nuclear localization signal in cellular retinoic acid binding protein-II. *Mol. Cell* **18**, 343-353

44. Zhu, J., Qiu, Z., Wiese, C., Ishii, Y., Friedrichsen, J., Rajashekara, G., and Splitter, G. A. (2005) Nuclear and mitochondrial localization signals overlap within bovine herpesvirus 1 tegument protein VP22. *J. Biol. Chem.* **280**, 16038-16044

45. Kahle, J., Baake, M., Doenecke, D., and Albig, W. (2005) Subunits of the heterotrimeric transcription factor NF-Y are imported into the nucleus by distinct pathways involving importin beta and importin 13. *Mol. Cell. Biol.* **25**, 5339-5354

46. Cansizoglu, A. E., Lee, B. J., Zhang, Z. C., Fontoura, B. M., and Chook, Y. M. (2007) Structure-based design of a pathway-specific nuclear import inhibitor. *Nat. Struct. Mol. Biol.* **14**, 452-454

47. Turpin, P., Ossareh-Nazari, B., and Dargemont, C. (1999) Nuclear transport and transcriptional regulation. *FEBS Lett.* **452**, 82-86

48. Majerciak, V., Yamanegi, K., Nie, S. H., and Zheng, Z. M. (2006) Structural and functional analyses of Kaposi sarcoma-associated herpesvirus ORF57 nuclear localization signals in living cells. *J. Biol. Chem.* **281**, 28365-28378

49. Friedrich, B., Quensel, C., Sommer, T., Hartmann, E., and Kohler, M. (2006) Nuclear localization signal and protein context both mediate importin alpha specificity of nuclear import substrates. *Mol. Cell. Biol.* **26**, 8697-8709

50. Rodriguez, M., Benito, A., Tubert, P., Castro, J., Ribo, M., Beaumelle, B., and Vilanova, M. (2006) A cytotoxic ribonuclease variant with a discontinuous nuclear localization signal constituted by basic residues scattered over three areas of the molecule. *J. Mol. Biol.* **360**, 548-557

51. Hara, M. R., Agrawal, N., Kim, S. F., Cascio, M. B., Fujimuro, M., Ozeki, Y., Takahashi, M., Cheah, J. H., Tankou, S. K., Hester, L. D., Ferris, C. D., Hayward, S. D., Snyder, S. H., and Sawa, A. (2005) S-nitrosylated GAPDH initiates apoptotic cell death by nuclear translocation following Siah1 binding. *Nat. Cell Biol.* **7**, 665-674

52. Pajares, M. A., Duran, C., Corrales, F., and Mato, J. M. (1994) Protein kinase C phosphorylation of rat liver S-adenosylmethionine synthetase: dissociation and production of an active monomer. *Biochem. J.* **303**, 949-955

53. Kramer, A., Ludwig, Y., Shahin, V., and Oberleithner, H. (2007) A pathway separate from the central channel through the nuclear pore complex for inorganic ions and small macromolecules. *J. Biol. Chem.* **282**, 31437-31443

54. Bhaumik, S. R., Smith, E., and Shilatifard, A. (2007) Covalent modifications of histones during development and disease pathogenesis. *Nat. Struct. Mol. Biol.* **14**, 1008-1016

55. Richards, E. J., and Elgin, S. C. (2002) Epigenetic codes for heterochromatin formation and silencing: rounding up the usual suspects. *Cell* **108**, 489-500

56. Shivapurkar, N., and Poirier, L. A. (1983) Tissue levels of S-adenosylmethionine and S-adenosylhomocysteine in rats fed methyl-deficient, amino acid-defined diets for one to five weeks. *Carcinogenesis* **4**, 1051-1057

57. Zhou, W., Alonso, S., Takai, D., Lu, S. C., Yamamoto, F., Perucho, M., and Huang, S. (2008) Requirement of RIZ1 for cancer prevention by methyl-balanced diet. *PLoS ONE* **3**, e3390

58. Radomski, N., Kaufmann, C., and Dreyer, C. (1999) Nuclear accumulation of S-adenosylhomocysteine hydrolase in transcriptionally active cells during development of Xenopus laevis. *Mol. Biol. Cell* **10**, 4283-4298

59. Jeffery, C. J. (1999) Moonlighting proteins. *Trends Biochem. Sci.* **24**, 8-11

ACKNOWLEDGEMENTS

E. R. Reytor was a fellow of RCMN C03/08, PI05/0563 and the I3P Program of the CSIC. The authors wish to thank Dr. E. Sanchez-Góngora and Dr. C. D. Pérez Ortega for preliminary experiments, Dr. Y. Labzecnik for providing the multiple EGFP vectors, Dr. J. E. Felíu for primary hepatocyte preparations, Dr. G Varela-Moreiras and T. Partearroyo for their help in DNA methylation assays and Dr. J. P. Garcia Ruiz for critical reading of the manuscript. This work was supported by grants of the Ministerio de Educación y Ciencia (BMC2002-0243 and BFU2005-00050 to MAP and SAF2006-03489 to DPS) and the Instituto de Salud Carlos III (RCMN C03/08 to MAP and RD07/0064/0007 to DPS).

FIGURE LEGENDS

Figure 1. MATα1 expression in rat tissues. Panel A shows a western blot of cytosolic fractions (80 μg per lane) from several rat tissues developed with anti-MAT I/III antiserum. Panel B includes preimmune (a, c, e, g, i and k) and immune staining (b, d, f, h, j and l) of tissue sections, where a discontinuous line indicates the contour of typical cells (the bar corresponds to

10 μm). Panel C shows RT-PCR results using specific primers for MAT1A (I) and MAT2A (II) amplification. Panel D presents data of real-time PCR for MAT1A mRNA in triplicate ± SD, using the kidney levels as reference for graphical purposes. Liver, pancreas and lung levels are significantly different from the rest of the tissues and between them according to Student's t-tests of the data ($p < 0.02$).

Figure 2. MATα1 constructs used in this work and their oligomeric structures. Panel A depicts a schematic view of the constructs used in this work, including the sequences of the C-terminal end of MATα1 and the linkers. Panel B shows a representative western blot (10 μg/lane) of MATα1 (lane 1), FLAG-MAT (lane 2) and MAT-EGFP (lane 3) expression in the soluble fraction of *E. coli* using anti-MAT I/III and anti-EGFP antibodies. The calculated molecular masses appear on the left side of the figure. Panel C shows the sequence of the last 97 residues of the C-terminal domain, indicating the position of the exposed basic amino acids (red), the positions at which stop codons were introduced (*) and the putative low score NES sequence (underlined). Panel D depicts views of the tetramer and dimer structures (subunits A and B in palecyan and salmon, respectively) highlighting the residues mutated in this work, as well as the 394-396 stretch.

Figure 3. Subcellular distribution of MATα1. Panel A shows in vivo expression of MAT-EGFP (left) and indirect immunofluorescence of FLAG-MAT using anti-FLAG (right) in different cell lines by confocal microscopy, as well as colocalization with nuclear staining (bar scale 25 μm). Panel B illustrates MAT-EGFP expression in the CHO Tet-On MAT-EGFP stable clone as a function of doxycycline concentration by both western blot and confocal microscopy

(bar scale 17 μm). Panel C includes preimmune and immune staining of hepatocytes using anti-MAT I/III antiserum, the overlap with nuclear staining appearing in white (bar scale 16 μm). Panel D shows a representative western blot of nuclear and cytoplasmic fractions obtained from COS-7 cells and hepatocytes developed with anti-FLAG, anti-EGFP or anti-MAT antibodies, as indicated. Anti-cJun and anti-α-Tubulin antibodies were used as nuclear and cytoplasmic markers, respectively. Average LDH activity in the nuclear fractions was < 0.8% of that in the cytosol.

Figure 4. Subcellular distribution of truncated forms and C-terminal fragments. Panel A shows a representative western blot of nuclear and cytoplasmic fractions (80 μg/lane) of FLAG-MAT truncated proteins expressed in COS-7 cells using anti-FLAG with their calculated masses appearing on the right. Confocal microscopy images of the truncated proteins (panel B, bar scale 15 μm) and the C-terminal fragments fused to pentameric EGFP (panel C, bar scale 25 μm) are also shown. Colocalization with Hoechst nuclear staining appears in white. Panel C also includes images of pentameric EGFP and the NLS-EGFP3x controls.

Figure 5. Distribution of mutant proteins in subcellular compartments. Panel A shows confocal microscopy images of CHO cells overexpressing the FLAG-MAT and MAT-EGFP mutants used in this study, the Hoechst overlapping nuclear signal appearing in white (bar scale 25 μm). FLAG-MAT signals were detected using anti-FLAG. Panel B includes representative western blots of COS-7 subcellular fractions for the mutants developed with anti-FLAG, anti-α-Tubulin and anti-TBP (TATA binding protein). Dotted lines indicate positions at which lanes

from this representative blot have been cropped. Average LDH activity in the nuclear fractions was < 0.8% of that in the cytosol.

Figure 6. MATα1 locates at the nuclear matrix. Nuclear matrix preparations of CHO cells expressing wild type, truncated and the F251D mutant of MATα1 were analyzed by confocal microscopy using anti-FLAG and anti-SC-35 antibodies. FLAG-MAT signals (green) overlap with SC-35 (red), a nuclear matrix marker, colocalization appearing in orange (bar scale 20 μm).

Figure 7. Nuclear MATα1 association state. Cotransfections of COS-7 cells with pFLAG-MAT and pMAT-EGFP or pFLAG-MAT and pEGFP as a control were performed to analyze the association state shown by MATα1 subunits in the nucleus. The figure shows inmunoprecipitation of FLAG-MAT followed by western blot detection of MAT-EGFP (panel A left) or EGFP (panel A right) of nuclear (N) and cytosolic (C) fractions using anti-EGFP. The expression of both types of MATα1 subunits, as well as the purity of the fractions, is demonstrated by western blot of the input samples using anti-FLAG and anti-EGFP antibodies. The purity of the subcellular fractions was analyzed using anti-cJun and anti-tubulin for detection of these nuclear and cytoplasmic markers, respectively. Average LDH activity in the nuclear fractions was < 0.8% of that in the cytoplasm. Panel B shows the gel filtration chromatography profile of nuclear extracts without detergents (LDH activity < 0.05% of that in the cytoplasm). The presence of MATα1 in the fractions was detected by Dot-blot (200 μl) using anti-MAT. The arrows indicate the elution position of tetramers (a) and monomers (b). The protein standards used and their elution volumes were as follows: Dextran Blue (2000 kDa), 8.69

ml; apoferritin (443 kDa), 9.87 ml; β-amylase (200 kDa), 11.34 ml; alcohol dehydrogenase (150 kDa), 12.07 ml; carbonic anhydrase (29 kDa), 15.12 ml; and ATP (0.551 kDa), 19.26 ml.

Figure 8. Effects of MATα1 overexpression on histone H3 trimethylation. FLAG-MAT and selected mutants were overexpressed in CHO cells to evaluate the impact exerted on histone H3 trimethylation levels at residues K4, K9 and K27 by western blot. Panel A shows the effect of wild type MAT overexpression as compared to the empty plasmid on these three methylations. Panel B shows the effects on K27 trimethylation of MAT mutants showing preferred cytoplasmic (R344A and K393) and nuclear localizations (K368A and K369A), as well as those of the inactive F251D mutant. The histograms show the mean of the results corrected against α-Tubulin (panel A) and MAT levels (panel B) of seven independent experiments ± SEM. The results were considered significant when $p < 0.05$ (*) according to the Student's t-test performed against pFLAG (panel A) and WT (panel B).

Table 1

Oligonucleotides used for mutagenesis. The table lists the oligonucleotides (sense only) used for mutagenesis in this work.

Mutated plasmid	Residue change	Primers (5'-3'; sense only)
pMAT-EGFP	**R313A**	GGCTGGGCTCTGCGCCAGAGTCCTTGTTC
	K340A	CCTACGGAACTTCCGCCAAGACTGAGCGAGAG
	K341A	CTACGGAACTTCCAAGGCCACTGAGCGAGAGC
	R344A	CCAAGAAGACTGAGGCAGAGCTACTAGAGG
	R357A	CAAGAACTTTGACCTCGCCCCGGGTGTTATTGTC
	R363A	CCGGGTGTTATTGTCGCCGACTTGGATCTGAAG
	K368A	GGGACTTGGATCTGGCCAAGCCCATCTACCAG
	K369A	GACTTGGATCTGAAGGCCCCCATCTACCAGAAG
	K374A	GCCCATCTACCAGGCCACTGCATGCTATGG
	K392A	CCTGGGAGGTCCCCGCCAAGCTTCGAATTC
	K393A	GGGAGGTCCCCAAGGCCCTTCGAATTCTGC
pFLAG-MAT	**R313A**	GGCTGGGCTCTGCGCCAGAGTCCTTGTTC
	K340A	CCTACGGAACTTCCGCCAAGACTGAGCGAGAG
	K341A	CTACGGAACTTCCAAGGCCACTGAGCGAGAGC
	R344A	CCAAGAAGACTGAGGCAGAGCTACTAGAGG
	R357A	CAAGAACTTTGACCTCGCCCCGGGTGTTATTGTC
	R363A	CCGGGTGTTATTGTCGCCGACTTGGATCTGAAG
	K368A	GGGACTTGGATCTGGCCAAGCCCATCTACCAG
	K369A	GACTTGGATCTGAAGGCCCCCATCTACCAGAAG
	K374A	GCCCATCTACCAGGCCACTGCATGCTATGG
	K392A	CCTGGGAGGTCCCCGCCAAGCTTGTGTTTTAG
	K393A	GGGAGGTCCCCAAGGCCCTTGTGTTTTAGAGC
	R313X	GGCTGGGCTCTGCTAGAGAGTCCTTGTTC
	N351X	GAGCTACTAGAGGTTGTGTGAAAGAACTTTGACCTCCG
	K393X	GGGAGGTCCCCAAGTAGCTTGTGTTTTAG

Table 2

Immunohistochemistry staining and subcellular distribution. The organs listed in the table were extracted from adult Wistar rats, fixed and analyzed by immunohistochemistry using preimmune (control) and anti MAT I/III antisera. The most relevant cell types showing positive (+) and negative (-) staining for MATα1 among cytoplasm and nuclei appear summarized in the table.

	Anti-MAT signal		
Organ/tissue type	**Structure/cell type**	**Cytoplasm**	**Nucleus**
Liver	Hepatocytes	+	+
Brain	Cerebellar Purkinje cells	+	+
Kidney	Epithelium of renal tubules	+	+
Lung	Bronchiolar epithelium	+	+
Epididymus	Spermatogenic epithelium	-	+
Digestive system	Mucosa	-	+
Pancreas	Pancreatic acini cells	+	+
Heart	Muscle cells	-	+
Skeletal muscle	Muscle cells	-	+
Blood vessels	Endothelium	-	-
Smooth muscle	Visceral and vascular wall	-	-
Connective tissue	Visceral and vascular wall	-	-

Table 3

Methionine adenosyltransferase activity of the protein variants used in this study.

All the protein variants used in this study were expressed in *E. coli* BL21(DE3) and the soluble fractions isolated to determine their activity and oligomerization state. The table shows activity results from a typical experiment carried out in triplicate ± SD, and the association state detected by gel filtration chromatography (T = tetramer and D = dimer).

Construction	MAT activity (nmol/min/mg)	Association level
pSSRL-T7N	21.8 ± 4.30**	T, D
pMAT-EGFP-T7N*	1.41 ± 0.01**	D
pFLAG-CMV4	0.51 ± 0.03	-
pFLAG-CMV4-MAT*	2.36 ± 0.10	D
pFLAG-CMV4-MAT R313A	3.89 ± 0.17	T
pFLAG-CMV4-MAT K340A	5.35 ± 0.22	T, D
pFLAG-CMV4-MAT K341A	3.07 ± 0.37	T, D
pFLAG-CMV4-MAT R344A	3.19 ± 0.09	T, D
pFLAG-CMV4-MAT R357A	1.30 ± 0.09	T
pFLAG-CMV4-MAT R363A	3.66 ± 0.10	T, D
pFLAG-CMV4-MAT K368A	1.39 ± 0.09	T, D
pFLAG-CMV4-MAT K369A	2.64 ± 0.30	T, D
pFLAG-CMV4-MAT K374A	3.63 ± 0.47	T, D
pFLAG-CMV4-MAT K392A	2.35 ± 0.03	T, D
pFLAG-CMV4-MAT K393A	1.12 ± 0.03	T, D
pFLAG-CMV4-MAT R313X*	0.62 ± 0.04	ND
pFLAG-CMV4-MAT N351X*	0.73 ± 0.04	ND
pFLAG-CMV4-MAT K393X*	0.86 ± 0.03	ND

* Proteins with low or very low expression levels.
** constructs needing IPTG induction.
ND, not determined

Figure 1

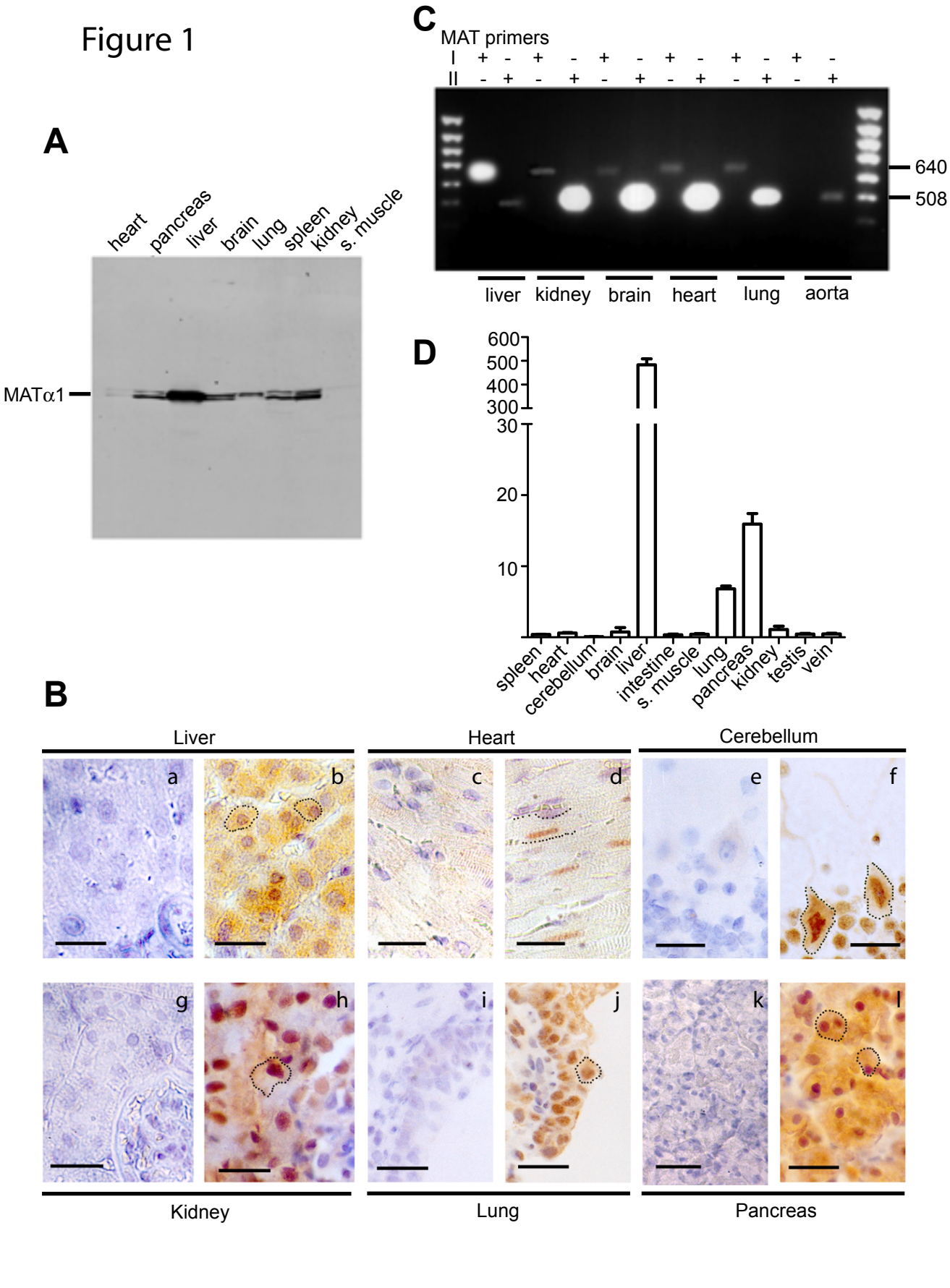
A
heart
pancreas
liver
brain
lung
spleen
kidney
s. muscle
MATα1
C
MAT primers
I + - + - + - + - + - + -
II - + - + - + - + - + - +
640
508
liver
kidney
brain
heart
lung
aorta
D
600
500
400
300
30
20
10
spleen
heart
cerebellum
brain
liver
intestine
s. muscle
lung
pancreas
kidney
testis
vein
B
Liver
Heart
Cerebellum
a
b
c
d
e
f
g
h
i
j
k
l
Kidney
Lung
Pancreas

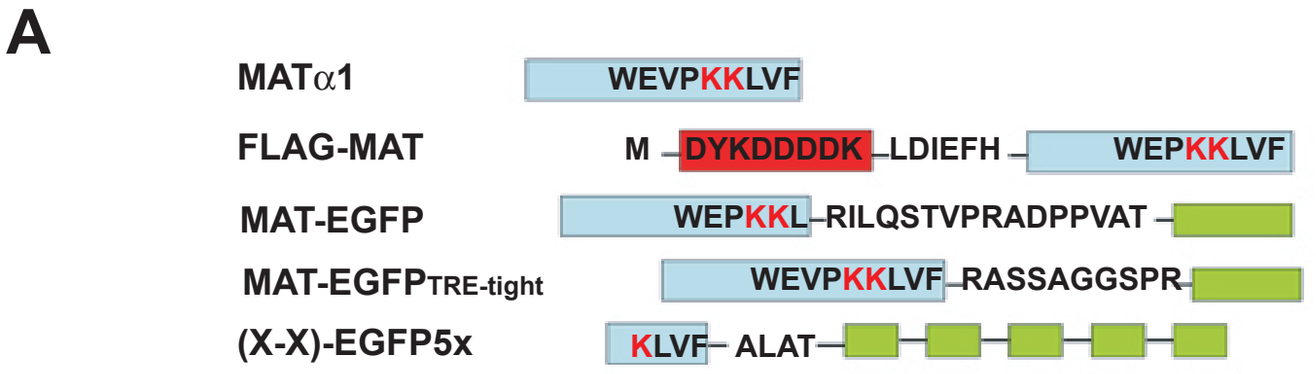

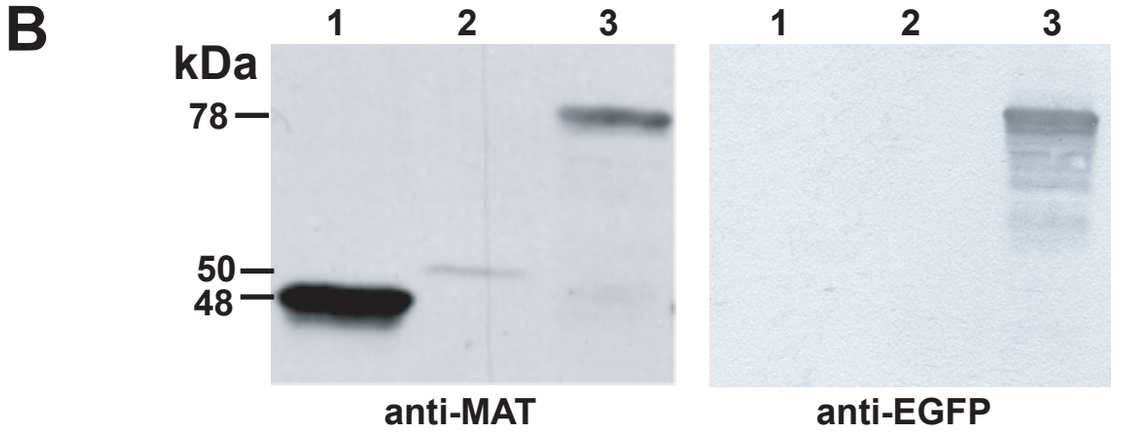

C

^{300}WVAKSLVKA ^{310}GLCRRVLVQV ^{320}SYAIGVAEPL ^{330}SISIFTYGTS

^{340}KKTERELLEV ^{350}VNKNFDLRPG ^{360}VIVRDLDLKK ^{370}PIYQKTACYG

^{380}HFGRSEFPWE ^{390}VPKKLVF^{396}

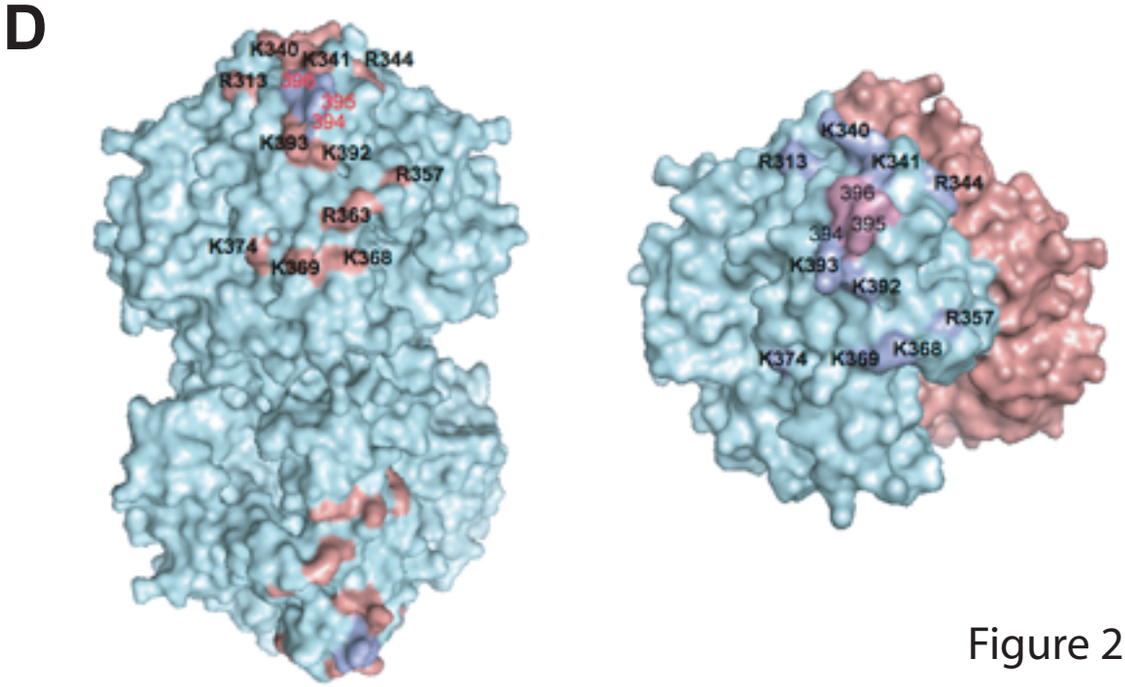

Figure 2

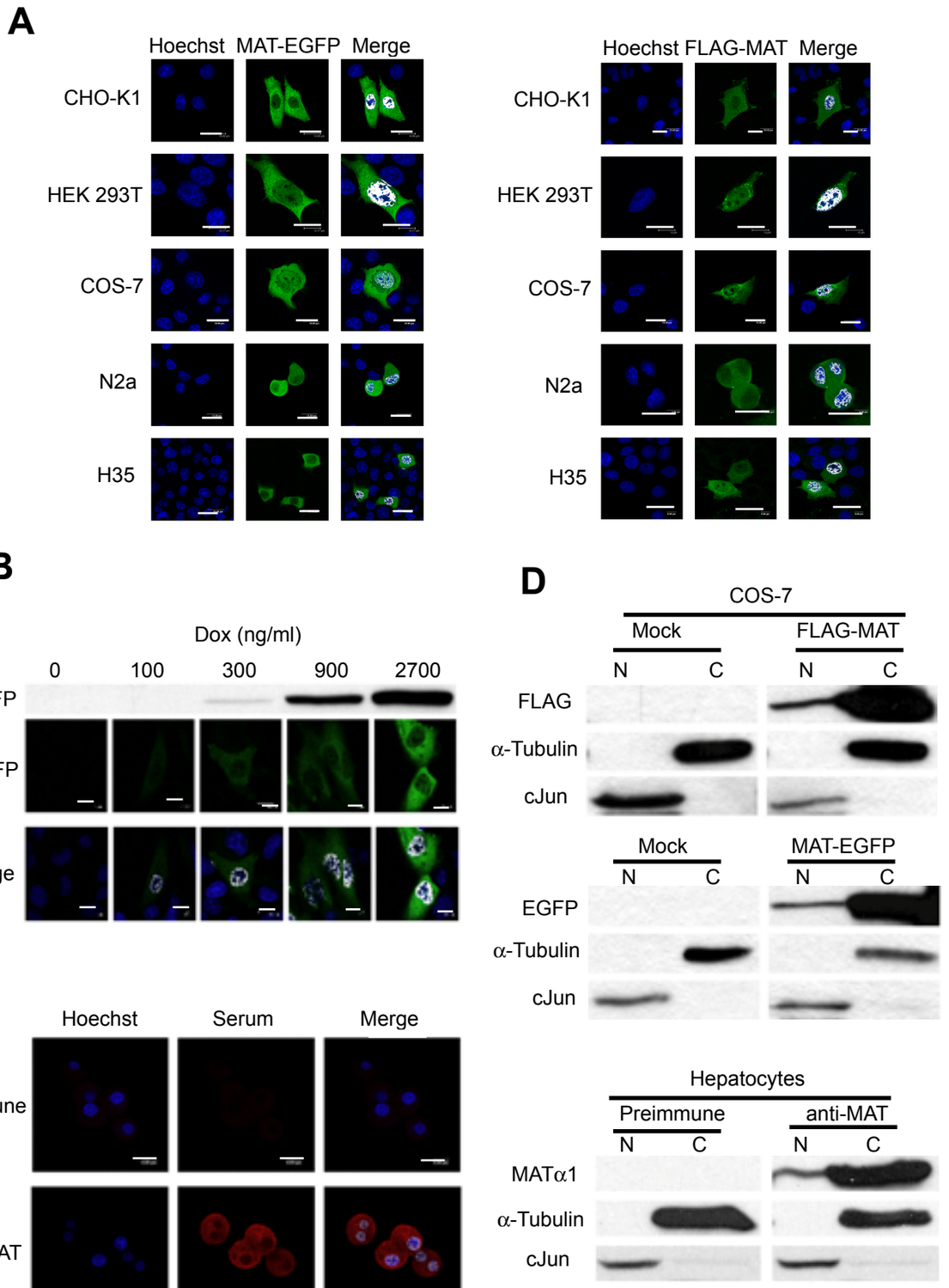
A
Hoechst
MAT-EGFP
Merge
CHO-K1
HEK 293T
COS-7
N2a
H35
Hoechst
FLAG-MAT
Merge
CHO-K1
HEK 293T
COS-7
N2a
H35
B
Dox (ng/ml)
0
100
300
900
2700
MAT-EGFP
MAT-EGFP
Merge
C
Hoechst
Serum
Merge
Preimmune
anti-MAT
D
COS-7
Mock
FLAG-MAT
N
C
N
C
FLAG
α-Tubulin
cJun
Mock
MAT-EGFP
N
C
N
C
EGFP
α-Tubulin
cJun
Hepatocytes
Preimmune
anti-MAT
N
C
N
C
MATα1
α-Tubulin
cJun

Figure 3

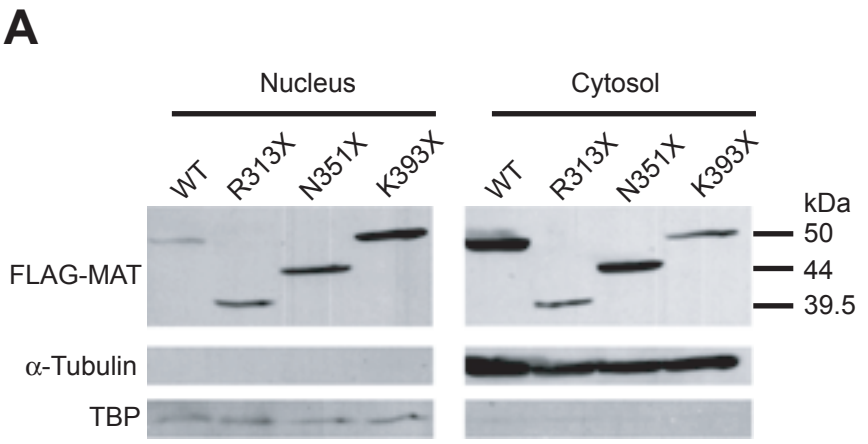
A
Nucleus
Cytosol
WT
R313X
N351X
K393X
WT
R313X
N351X
K393X
kDa
50
44
39.5
FLAG-MAT
α-Tubulin
TBP

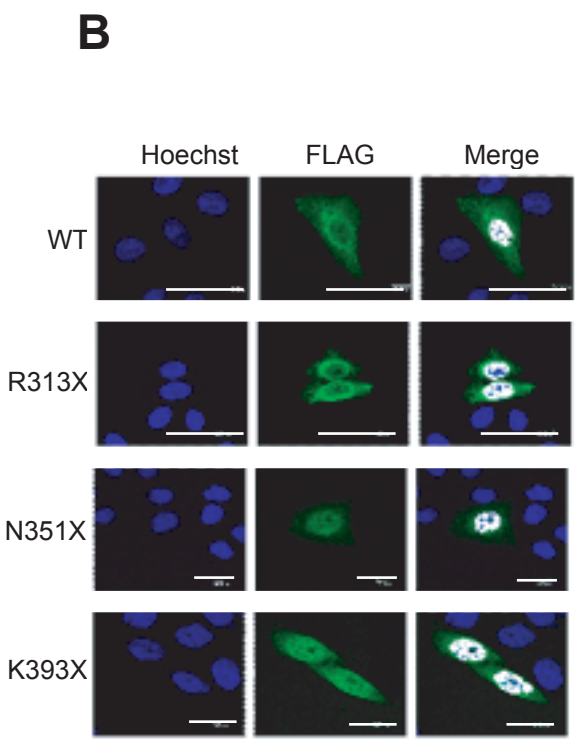
B
Hoechst
FLAG
Merge
WT
R313X
N351X
K393X

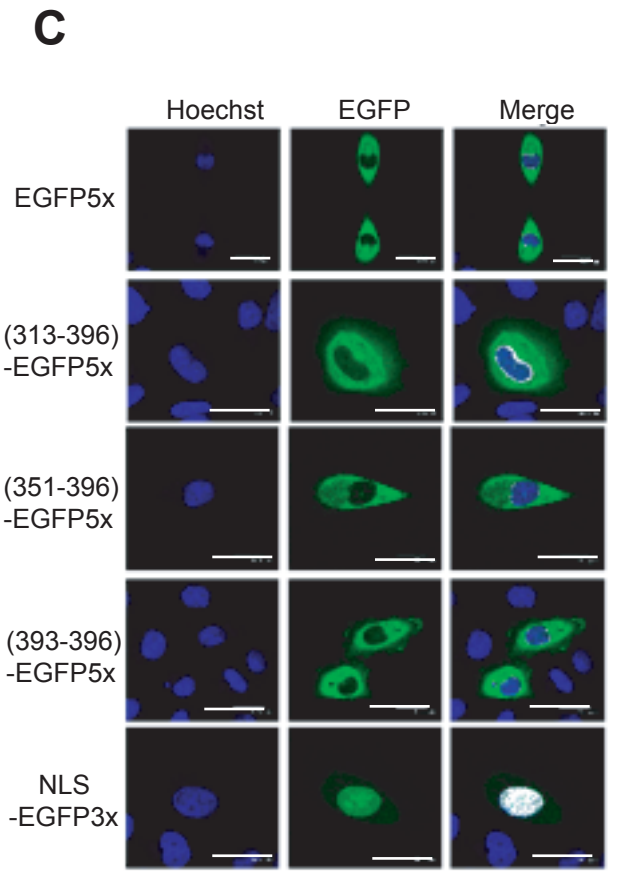
C
Hoechst
EGFP
Merge
EGFP5x
(313-396)
-EGFP5x
(351-396)
-EGFP5x
(393-396)
-EGFP5x
NLS
-EGFP3x

Figure 4

Figure 5

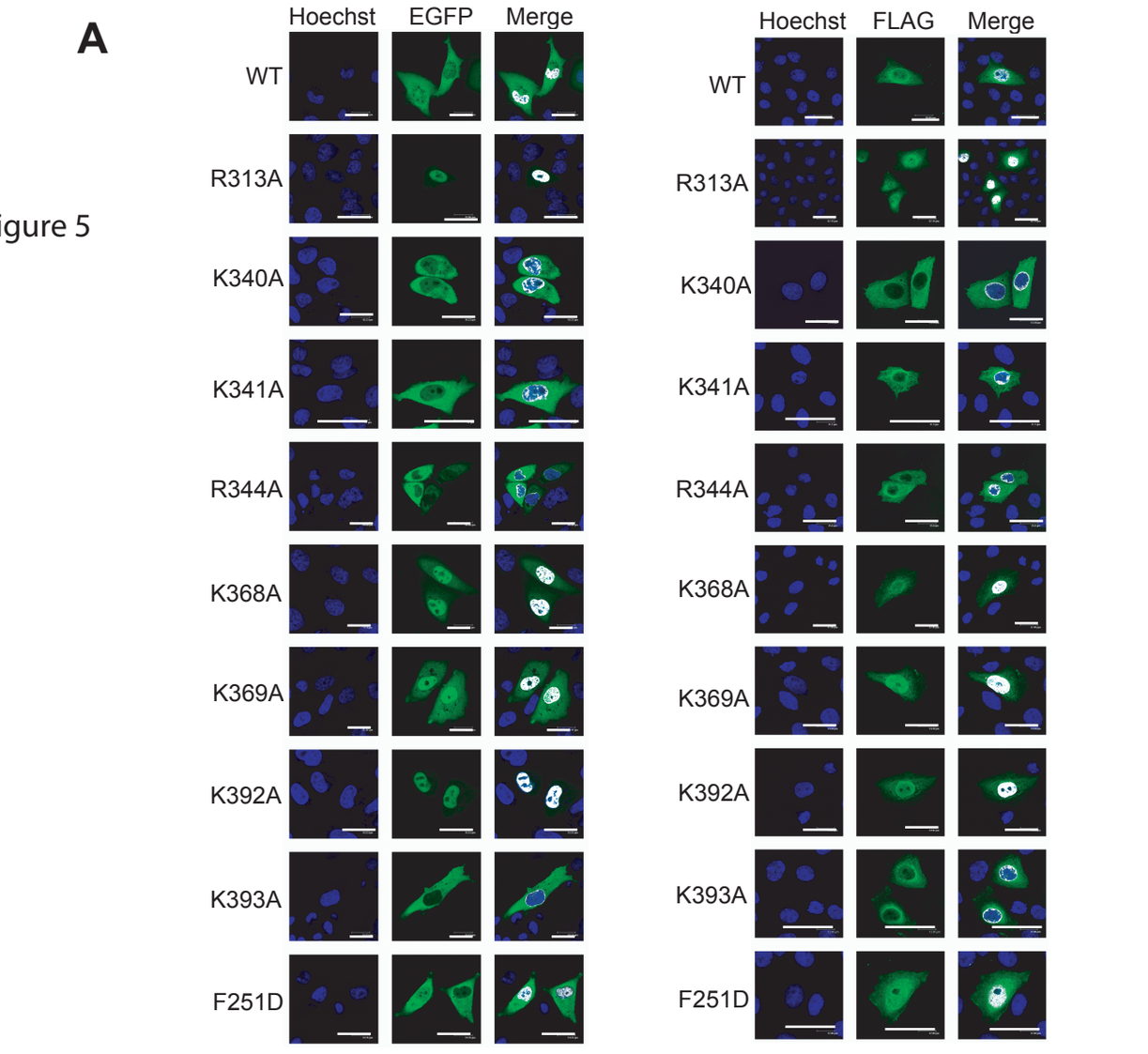
A
Hoechst
EGFP
Merge
Hoechst
FLAG
Merge
WT
R313A
K340A
K341A
R344A
K368A
K369A
K392A
K393A
F251D
B
R313A
K340A
K341A
R344A
K368A
K369A
K392A
K393A
WT
F251D
WT
Nucleus
FLAG-MAT
α-Tubulin
TBP
Cytosol
FLAG-MAT
α-Tubulin
TBP

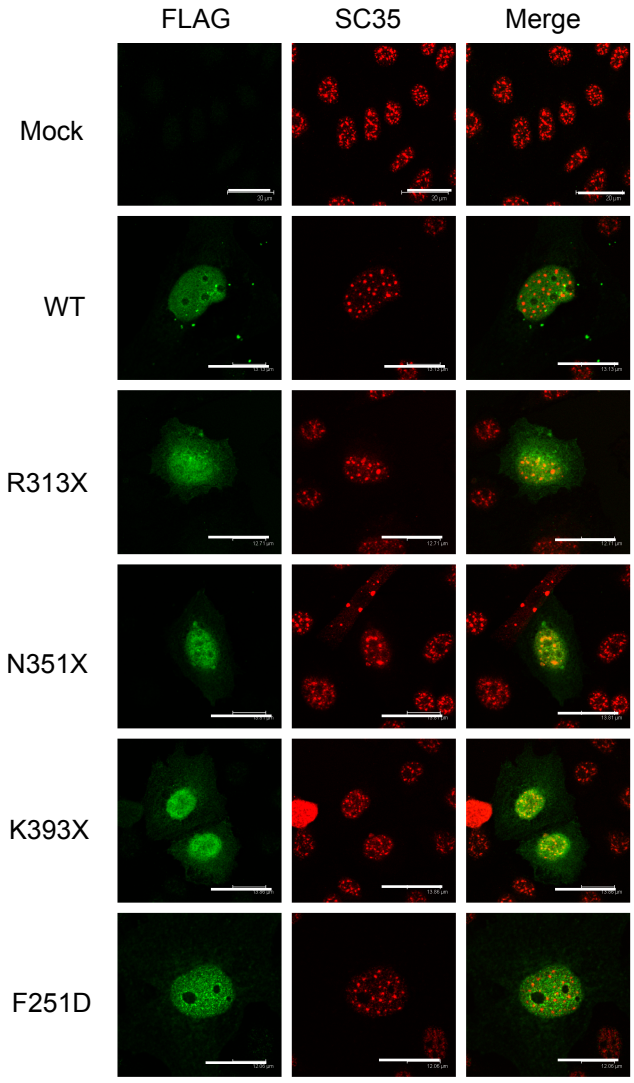

Figure 6

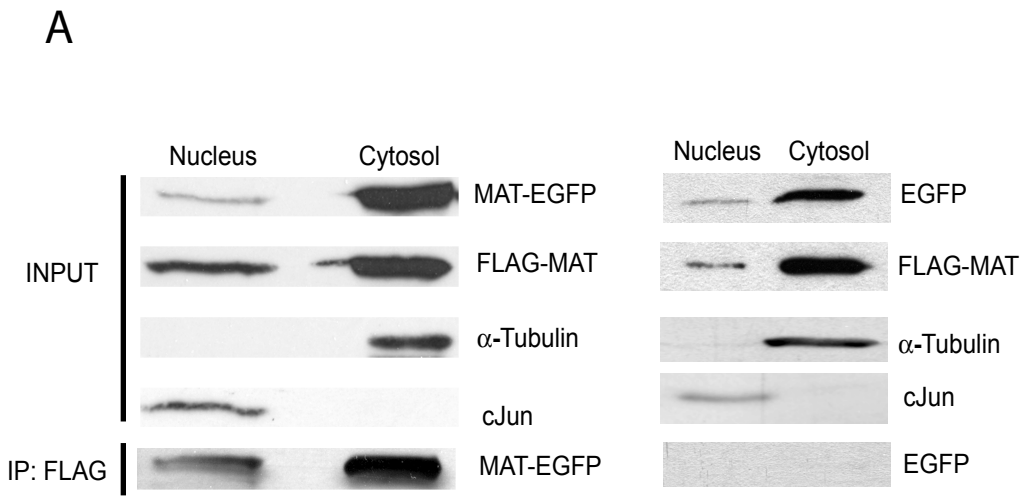
A
Nucleus
Cytosol
Nucleus
Cytosol
INPUT
MAT-EGFP
EGFP
FLAG-MAT
FLAG-MAT
α-Tubulin
α-Tubulin
cJun
cJun
IP: FLAG
MAT-EGFP
EGFP

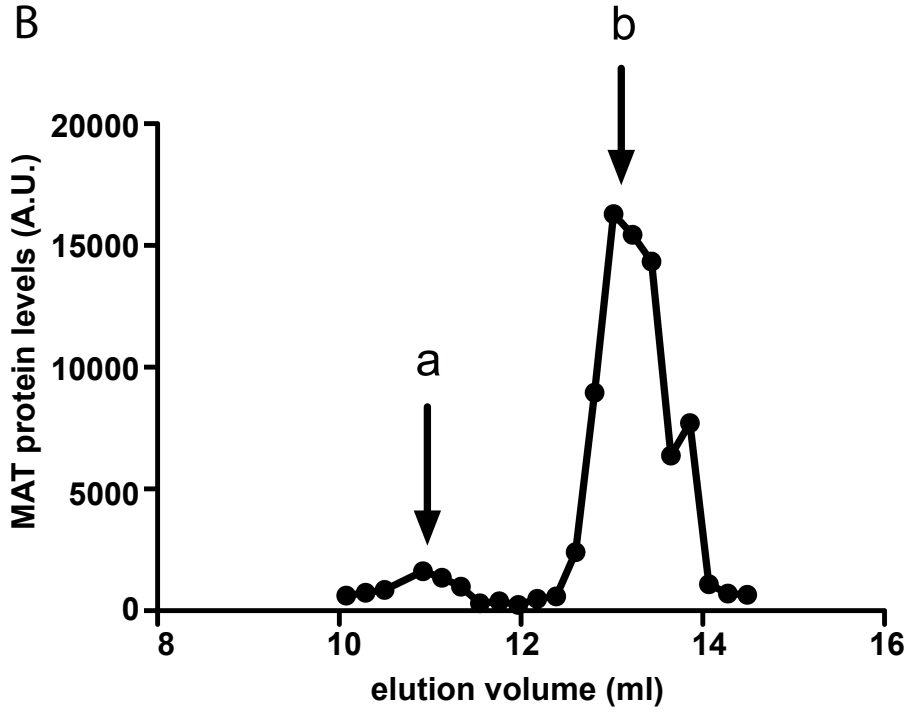
B
b
a
20000
15000
10000
5000
0
MAT protein levels (A.U.)
8
10
12
14
16
elution volume (ml)

Figure 7

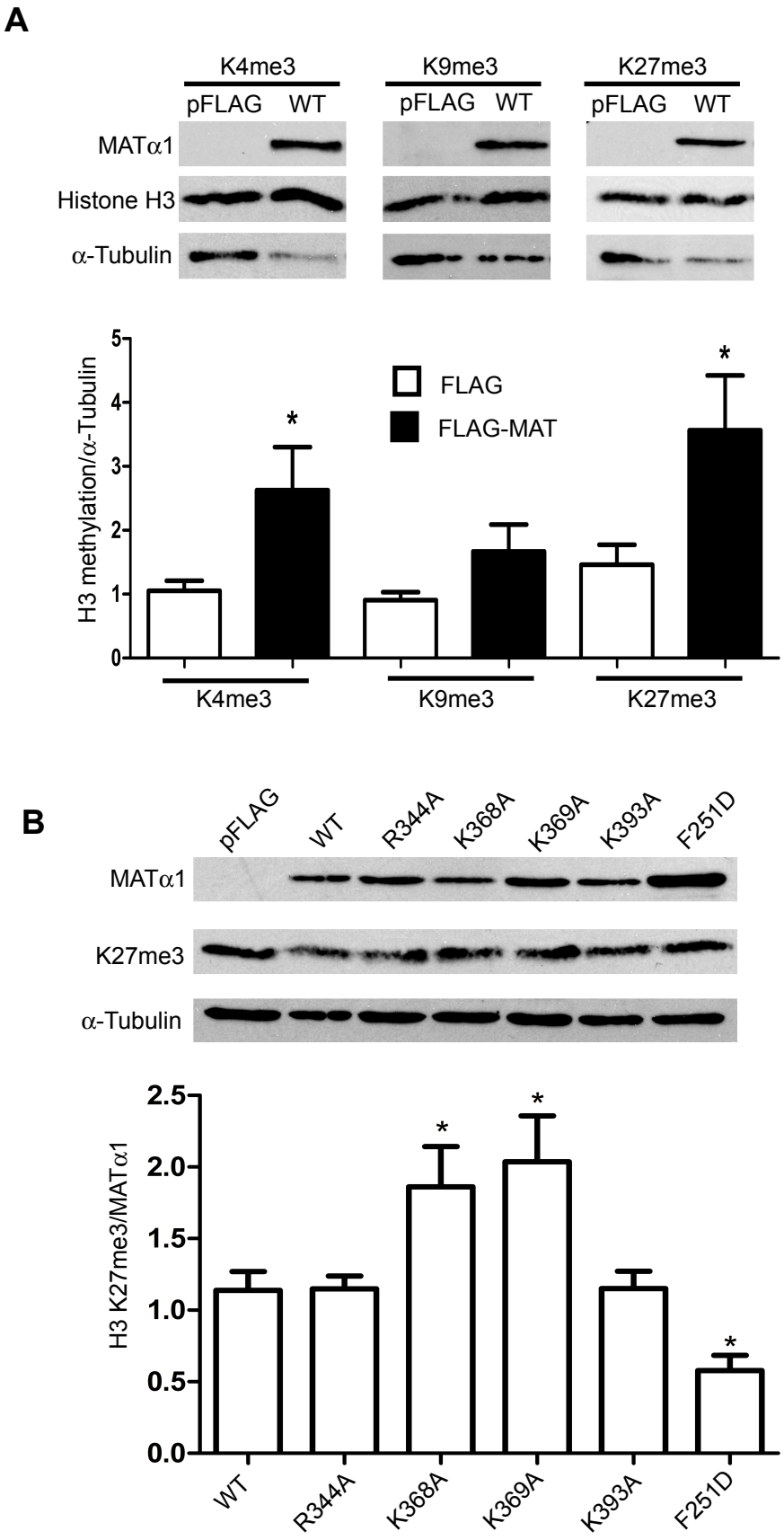
A
K4me3
K9me3
K27me3
pFLAG
WT
MATα1
Histone H3
α-Tubulin
H3 methylation/α-Tubulin
FLAG
FLAG-MAT
K4me3
K9me3
K27me3
B
pFLAG
WT
R344A
K368A
K369A
K393A
F251D
MATα1
K27me3
α-Tubulin
H3 K27me3/MATα1
WT
R344A
K368A
K369A
K393A
F251D

Figure 8